

MSc. Thesis

**SIMULTANEOUS CALIBRATION OF A  
STRUCTURED LIGHT-BASED  
CATADIOPTIC STEREO SENSOR**

by

**DIEU SANG LY**

Supervisors:

Pr. EL MUSTAPHA MOUADDIB

Dr. JOAQUIM SALVI

A Thesis submitted for the Degree of  
MSc Erasmus Mundus in Computer Vision and Robotics (VIBOT)

– 2008 –

## Abstract

The omnidirectional vision systems enlarge the field of view of conventional cameras by means of special lenses, multi-image acquisition systems or catadioptric cameras. The catadioptric cameras are the customary ones coupled with mirrors of special curvatures to obtain an entire field of view. Structured light projection is widely used to solve the correspondence problem in stereo computation. This thesis is focused on a structured light-based stereo system which is formed by a catadioptric camera and an omnidirectional laser projector.

Calibration is a critical process before using a camera for any further purpose. Therefore over the past decades, many researches have been dedicated to calibration methods for omnidirectional vision sensors in order to achieve efficient approaches. In the most recent work on catadioptric stereo system based on structured light projection, the catadioptric camera and the omnidirectional laser projector are calibrated sequentially to estimate the parameters of each component. This thesis proposes a novel calibration which permits a simultaneous calibration for both of them. The proposed method simplifies the process of sequential calibration while preserving the accuracy of the scene reconstruction. Particularly the simultaneous approach provides an important improvement when it does not require an accurate measurement of the calibration patterns in 3D space as the sequential approach does.

After the sensor parameters are estimated, the sensor model can be used for depth measurement which has many further applications such as scene reconstruction, robot navigation, etc.

**Keywords:** omnidirectional vision, parabolic mirror, structured light, stereo vision.

*Ose rêver. Ose essayer. Ose te tromper. Ose avoir du succès. Vas-y. Je te lance un défi!*

Kingsley Ward

# Contents

<b>Acknowledgements</b>	<b>v</b>
<b>1 Introduction</b>	<b>1</b>
1.1 Omnidirectional vision . . . . .	1
1.1.1 Special lenses . . . . .	2
1.1.2 Multi-image acquisition systems . . . . .	2
1.1.3 Catadioptric cameras . . . . .	3
1.2 Catadioptric cameras . . . . .	3
1.3 Stereo vision systems with catadioptric cameras . . . . .	7
1.4 Structured light projection in stereo vision systems . . . . .	11
1.5 Structured light-based catadioptric stereo sensors . . . . .	12
1.6 Objectives . . . . .	13
1.7 Thesis outline . . . . .	14
<b>2 Problem Definition</b>	<b>15</b>
<b>3 State of the Art: Sequential Calibration</b>	<b>17</b>
3.1 Arrangements of a structured light-based catadioptric stereo sensor . . . . .	17
3.2 Sequential calibration of structured light-based catadioptric stereo sensor . . . . .	19
3.2.1 Catadioptric camera calibration using equivalent projection of a sphere . . . . .	19
3.2.2 Omnidirectional laser projector calibration . . . . .	21

<b>4</b>	<b>Novel Approach: Simultaneous Calibration</b>	<b>25</b>
4.1	Sensor modelling . . . . .	25
4.2	Simultaneous calibration . . . . .	28
4.3	Comparison of the sequential and simultaneous calibrations . . . . .	29
4.3.1	Sequential calibration . . . . .	30
4.3.2	Simultaneous calibration . . . . .	33
<b>5</b>	<b>Experimental Results</b>	<b>35</b>
5.1	Comparison of two calibration methods . . . . .	35
5.2	Combination of two calibration methods . . . . .	38
<b>6</b>	<b>Conclusions</b>	<b>41</b>
6.1	Conclusions . . . . .	41
6.2	Future works . . . . .	42
	<b>Bibliography</b>	<b>45</b>

# List of Figures

1.1	Nikkor 6mm fish-eye lens mounted on a Nikon F3 body . . . . .	2
1.2	RingCam omnidirectional sensor . . . . .	3
1.3	Hand with reflection sphere (1935) by M.C. Escher . . . . .	4
1.4	Omnidirectional sensor with planar mirror . . . . .	5
1.5	SYCLOP omnidirectional sensor with conical mirror . . . . .	5
1.6	Omnidirectional sensor with hyperboloidal mirror . . . . .	6
1.7	Omnidirectional sensor with paraboloidal mirror . . . . .	7
1.8	Epipolar geometry of two central catadioptric sensors with hyperboloidal mirrors	8
1.9	Catadioptric stereo systems proposed by Nene and Nayar . . . . .	8
1.10	Stereo system with two catadioptric video cameras . . . . .	9
1.11	Catadioptric stereo systems proposed by Ollis . . . . .	10
1.12	Stereo vision by structured light projection . . . . .	11
1.13	Structured light-based catadioptric stereo sensor . . . . .	12
1.14	ANIS robot . . . . .	13
3.1	Arrangements of a catadioptric camera and an omnidirectional laser projector . .	18
3.2	Sphere of equivalent model . . . . .	20
3.3	Calibration patterns . . . . .	21
3.4	Omnidirectional projection of a structured light . . . . .	23
3.5	Intersections of the cone of laser projection with calibration planes . . . . .	23

3.6	Laser stripes in catadioptric image . . . . .	23
4.1	Modelling of structured light-based catadioptric stereo sensor . . . . .	27
4.2	Geometry of an optical ray in the cone of projected laser pattern . . . . .	28
4.3	Synthetic laser points . . . . .	30
5.1	Reconstruction errors of the sequential and simultaneous calibrations with a surrounding environment of small range . . . . .	36
5.2	Reconstruction errors of the sequential and simultaneous calibrations with a surrounding environment of large range . . . . .	37
5.3	Reconstruction errors of two calibrations using 3D points approximated from the scene structure with a surrounding environment of large range . . . . .	38
5.4	Reconstruction errors of the sequential and simultaneous calibrations when combining these two approaches with a surrounding environment of small range . . .	39
5.5	Reconstruction errors of the sequential and simultaneous calibrations when combining these two approaches with a surrounding environment of large range . . .	39

# Acknowledgements

First of all, I would like to thank Mr. El Mustapha Mouaddib, my thesis director, for offering me an opportunity to work in the MIS laboratory, one of the pioneers in the field of omnidirectional vision. During three months of the thesis, he has shared with me his experience, his passion for research and especially he has been very patient with my French. Thanks to his thorough instruction, I did make much progress in my thesis.

Special thank to Mr. Joaquim Salvi, my second thesis director, for leading me to this research field and for the helpful advice he has given me during my period of research.

I would like to show my gratitude to the teaching staffs of Heriot Watt University, Universitat de Girona and Université de Bourgogne who have brought me much helpful knowledge as well as research experience during the Master.

I should also mention my gratefulness to Pascal, Cédric, Guillaume and Ali for their kindness during my stay in Amiens.

I will not forget Vibotian friends who have been next to me for three semesters and encouraged me when I had difficulties.

Finally, I want to express my deep gratitude and love to my family in my hometown.

# Chapter 1

## Introduction

This chapter is aimed to provide an overview on omnidirectional vision devices together with their characteristics. Next, several stereo vision systems using omnidirectional cameras are introduced. In addition, the readers will find a description of the structured light projection technique applied to omnidirectional stereo sensors. Finally, the objectives of this thesis are presented and the chapter is ended with the thesis outline.

### 1.1 Omnidirectional vision

Omnidirectional vision describes the perception of a vision system that can image the surroundings in all directions. An ideal omnidirectional camera should have a field of view of a sphere in 3D space which extends to infinity. However, it is physically impossible to manufacture this kind of camera; hence the possible solution is a vision sensor that has a field of view as wide as possible. There exist several devices capable of enlarging the field of view of conventional cameras, most of which can be divided into three main groups as follows:

- Special lenses (fish-eye lenses)
- Multi-image acquisition systems
- Catadioptric cameras

A desirable property of the omnidirectional sensors is the single viewpoint constraint. The central viewpoint systems only measure the intensity of light passing through a single point in 3D space, the projection point. The single viewpoint constraint permits the mapping of an omnidirectional image from the viewpoint to a perspective image, which is more perceptible, without distortion.

An entire class of omnidirectional vision systems has been analysed in [Nayar, 1997] and is summarized in the following sections.

### 1.1.1 Special lenses

Fish-eye lenses have shorter focal length and hence enable wider field of view than traditional lenses. However it is difficult to design the fish-eye lenses verifying the single viewpoint constraint and their field of view is often less than 180 degrees. In order to capture a hemi-spherical or wider view, the fish-eye lenses must be large and complex, and therefore expensive. It is possible to obtain a complete sphere of view by placing two fish-eye lenses back-to-back, yet this arrangement does not produce a single viewpoint.



Figure 1.1: Nikkor 6mm fish-eye lens mounted on a Nikon F3 body (photos by Jarle Aasland, left, and Kazuo Koga)

### 1.1.2 Multi-image acquisition systems

The panoramic view of the surrounding scene can be generated using multiple cameras looking at different directions. These cameras are arranged such that they have overlapped fields of view. This overlapping allows the sequence of captured images to be merged together to build the panoramic view of the scene. The main advantage is the high resolution of the panoramic image. However, the multi-camera systems do not possess a single viewpoint as each individual lens has its own projection centre. Moreover, the image processing power is necessary not only for the fusing of images but also for the interpretation of the combined panoramic one which is more detailed. Another solution for multi-image acquisition is to use a single camera rotating

about its projection centre. The rotating camera must be controlled accurately so that it is fast enough to capture the successive views of the scene in a short amount of time and slow enough to ensure that the images are not missed or blurred. It is evident that the imaging using such rotating device is delayed; hence it is not suitable for applications requiring instantaneous acquisition.

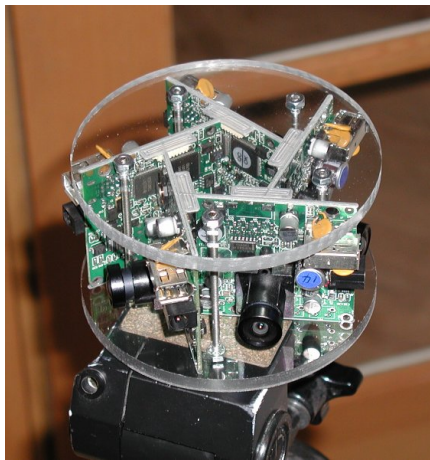


Figure 1.2: RingCam omnidirectional sensor. Courtesy of Ross Cutler (<http://research.microsoft.com/~rcutler/>)

### 1.1.3 Catadioptric cameras

The term catadioptric comes from dioptric, the science of light refraction (lenses) and catoptric, the science of reflective surfaces (mirrors). Catadioptric cameras combine the conventional cameras with mirrors to enlarge the field of view. These sensors can provide a 360 degree field of view and satisfy the single viewpoint constraint using mirrors of special shapes. However, these devices generate images of non-uniform resolution and the catadioptric images are less detailed than those obtained by multi-camera systems.

## 1.2 Catadioptric cameras

### Original ideas:

The idea of using reflective surfaces to observe the surrounding scene is not new. A classical example is the drawing of the Dutch graphic artist M.C. Escher (1898-1972) in which the painter drew his hand holding a reflecting sphere.



Figure 1.3: Hand with reflection sphere (1935) by M.C. Escher

The original catadioptric sensor has been initially proposed by Rees in 1970. In the US patent [Rees, 1970], Rees proposed the use of a hyperboloidal mirror to capture catadioptric images which could be mapped to traditional perspective ones. Twenty years later, Yagi and Kawato generated an omnidirectional camera using a conical mirror [Yagi and Kawato, 1990]. The sensor, namely COPIS (CONical Projection Image Sensor), was mounted on a mobile robot and used to capture the indoor scene. Afterwards, Hong and others studied the catadioptric sensor with a spherical mirror [Hong et al, 1991]. In 1993, Yamazawa and his colleagues employed again a hyperboloidal mirror in their omnidirectional sensor [Yamazawa et al, 1993]. In 1997, Nayar and Baker developed an ideal omnidirectional vision sensor combining a paraboloidal mirror and a telecentric lens [Nayar and Baker, 1997]. During the past decade, omnidirectional vision has been growing continuously as a great deal of researches in computer vision have been dedicated to omnidirectional sensors.

In [Baker and Nayar, 1999], Baker and Nayar have derived a complete class of single-lens single-mirror catadioptric sensors having a single viewpoint with reference to omnidirectional

systems that have been proposed in literature.

### 1. Planar mirror

The field of view can not be widened by a single planar camera. Moreover, the sensor built by a single camera and multiple planar mirrors does not enhance the field of view while still satisfying the single viewpoint constraint. Nalwa [1996] has developed a single viewpoint system by a pyramidal arrangement of 4 planar mirrors together with 4 conventional cameras, each of which looks at one of the mirrors.

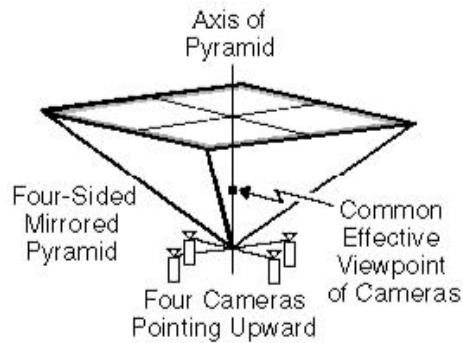


Figure 1.4: Omnidirectional vision sensor with four planar mirrors and four cameras proposed by Nalwa

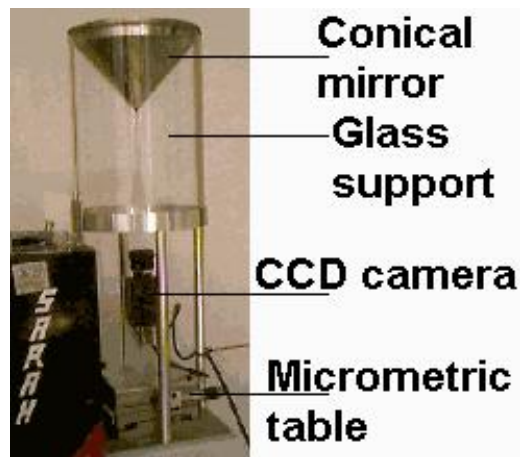


Figure 1.5: SYCLOP omnidirectional sensor with conical mirror. Courtesy of Cyril Cauchois (<http://www.iut-amiens.fr/~cauchois/>)

### 2. Conical mirror

The single viewpoint condition can be fulfilled by using a conical mirror as long as the camera pinhole resides at the apex of the cone. This configuration has been used several times [Yagi and Kawato, 1990], [Yagi and Yachida, 1991] and [Bogner, 1995], but in these experiments, the pinhole was at some distance from the apex of the cone. It was pointed out by [Nalwa, 1996] that if the pinhole moves away from the apex along the axis of the cone, the viewpoint is no longer a point but rather lies on a circular locus. The conical mirror was also applied in the SYCLOP (Conical SYstem for LOcalization and Perception) sensor by researchers at University of Picardie Jules Verne, leaded by Mouaddib [Pegard and Mouaddib, 1996].

### 3. Spherical mirror

The single effective viewpoint is achieved when the viewpoint and the pinhole coincide at the centre of the sphere. The spherical mirror and camera combination has been employed a number of times [Hong et al, 1991], [Bogner, 1995] and [Murphy, 1995] in which the pinhole was placed outside the sphere.

### 4. Ellipsoidal and hyperboloidal mirrors

The ellipsoidal and hyperboloidal mirrors satisfy the fixed view point constraint when the viewpoint and the pinhole are located at two foci of the ellipsoid and the hyperboloid respectively. The hyperboloidal mirror has been first used with a perspective lens by [Rees, 1970] to achieve a single viewpoint imaging system. Later, Yamazawa and others have implemented this configuration for autonomous navigation [Yamazawa et al, 1993].



Figure 1.6: Omnidirectional sensor using a hyperboloidal mirror in front of a perspective camera. Courtesy of Yagi, University of Osaka, Japan

### 5. Paraboloidal mirrors

A single viewpoint catadioptric sensor can be composed of a paraboloidal mirror and an or-

thographic camera. The main advantages of using an orthographic camera are the easier calibration and that the mirror can be translated arbitrarily whilst satisfying the single viewpoint constraint. The calibration is simpler because the paraboloidal mirror of any size can be used as long as the direction of the orthographic projection remains parallel to the symmetric axis of the mirror. One of the original ideas of using paraboloidal mirror was proposed by Nayar in 1997 [Nayar, 1997].



Figure 1.7: Omnidirectional sensor using paraboloidal mirror proposed by Nayar in 1997 with a hemispherical view (left) and entire sphere of view (right)

### 1.3 Stereo vision systems with catadioptric cameras

Stereo technique is used to obtain the range information of the scene from its images captured by cameras at different points of observation. This technique computes the location of each point in the scene from its projections in two or more images. The projections of a point in different images must be matched together to allow the depth estimation. The time-consuming matching can be speeded up by using epipolar geometry which permits the searching of the match of a point along the epipolar line instead of over the whole image. Since the epipolar geometry is a property of central projection cameras, it also exists for central catadioptric cameras. [Svoboda and Pajdla, 2002] introduced the epipolar geometry between two catadioptric sensors using parabolic, hyperbolic or elliptic mirrors.

Nene and Nayar proposed the catadioptric sensors for stereo computation using a single camera pointing towards multiple mirrors instead of two cameras frequently used in conventional stereo systems [Nene and Nayar, 1998]. Four configurations of mirrors in figure 1.9 have been

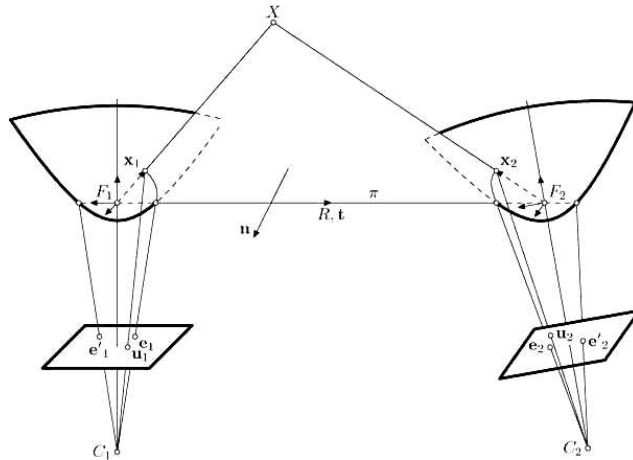


Figure 1.8: Epipolar geometry of two central catadioptric sensors with hyperboloidal mirrors

experimented:

(a) Two planar mirrors at an angle produce two effective viewpoints  $v$  and  $v'$  when imaged by a perspective (pinhole) camera  $p$ .

(b) Ellipsoidal mirrors are placed such that one focus of each of the mirrors coincides with the pinhole. The effective viewpoints are located at the other foci.

(c) Hyperboloidal mirrors are placed such that the exterior focus of each mirror coincides with the pinhole. The effective viewpoints are located at the other foci.

(d) Paraboloidal mirrors are placed such that their axes are parallel to each other. When imaged orthographically, the effective viewpoints are located at the interior foci.

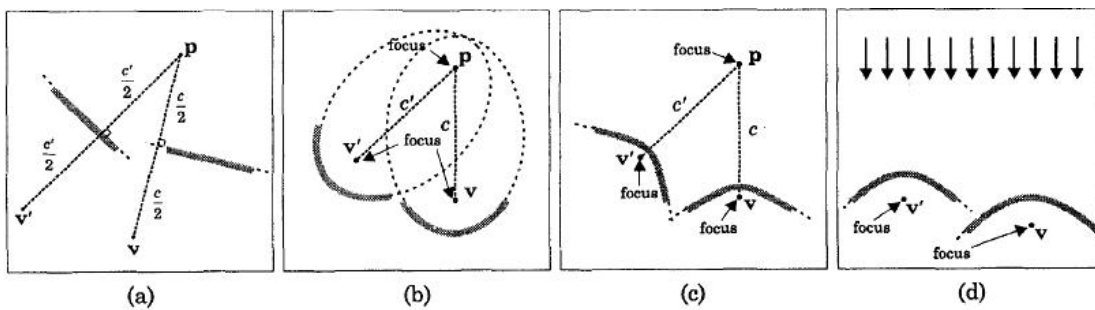


Figure 1.9: Four configurations of catadioptric stereo systems proposed by Nene and Nayar: (a) angled planar mirrors, (b) rotated ellipsoidal mirrors, (c) rotated hyperboloidal mirrors and (d) displaced paraboloidal mirrors

The authors also derived the epipolar constraints in each of these arrangements. The ad-

vantages of the proposed systems are wide field of view, single viewpoint projection, identical camera parameters, ease of calibration and lower cost compared to stereo systems using two or more cameras.

Gluckman and others introduced in [Gluckman et al, 1998] the panoramic stereo system composed of two vertically aligned (coaxial) paracatadioptric sensors, each of which combines an orthographic camera with a parabolic mirror (see figure 1.10) and hence verifies the single viewpoint constraint.



Figure 1.10: Stereo system with two catadioptric video cameras. Courtesy of Gluckman ([http://www1.cs.columbia.edu/CAVE/projects/cad\\_stereo/](http://www1.cs.columbia.edu/CAVE/projects/cad_stereo/))

This configuration has two main improvements. First, the singularities where depth can not be computed near the epipoles occur where the cameras occlude themselves. Second, the corresponding features in omnidirectional images belong to parallel epipolar lines; therefore this arrangement allows the real-time stereo processing. During the calibration step, the radii and the centres of the parabolas are determined by circle fitting in each image and the rotation between two cameras is estimated from manually selected corresponding points in two images. Unlike the epipolar geometry in the conventional stereo systems, the epipolar lines in a pair of coaxial omnidirectional images are radial lines and become parallel when the images are projected onto cylindrical panoramic images. After solving the corresponding problem, the depth of the scene can be computed by triangulation. Especially, depth computation does not depend on the focal length of the camera due to orthographic projection in each sensor.

Later, Ollis and others [Ollis et al, 1999] simulated different catadioptric stereo systems with two hyperbolic mirrors and one or two cameras as illustrated in figure 1.11.

Configuration 1: Both mirrors have similar curvatures, hence same resolution. This con-

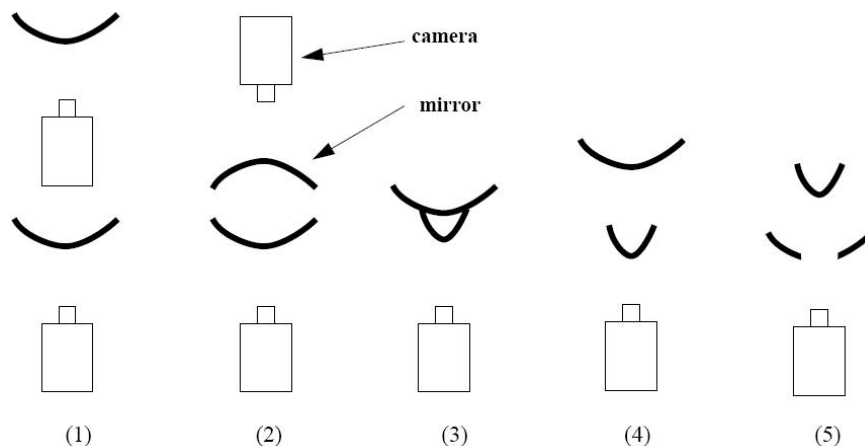


Figure 1.11: Side view of five configurations experimented by Ollis: (1) and (2) use two cameras, (3) to (5) use one camera

figuration provides the best range precision among the others. The range precision is easily controlled by adjusting the distance between two camera-mirror sets. This adjustment is more difficult for the single-camera multi-mirror systems in which the only possibility is to change the distance between the camera and the mirrors; which means that it is necessary to modify the mirror curvatures. The drawbacks are the cost of using two cameras and the calibration necessary for both cameras.

Configuration 2: The overlap of two fields of view is small and limited to the peripheries of two mirrors. Moreover, the distance between two mirrors is so short that the baseline of range calculation is quite limited compared to the dimension of the scene to be measure.

Configuration 3: A single camera is combined with a mirror of two curvatures. This configuration reduces the cost, the mechanical infrastructure and the calibration. However, a part of the view of the upper mirror is occluded by the lower mirror. In addition, the two mirrors are placed so close together that the baseline for the triangulation is limited.

Configuration 4: From configuration 3, the two lobes of the mirror are separated to increase the baseline. This configuration is more advantageous compared to the others except the first one.

Configuration 5: A convex mirror is placed above another mirror with a hole in the middle. With this configuration, both the precision and the depth maps are improved. However, the different resolutions of two mirrors are not well matched as those in configuration 3.

The feature matching is done by correlating a window in one image and another window along the epipolar line in the other image. A test has shown that ignoring the distortion caused

by the mirrors and using the standard window for the correlation introduce important inaccuracies in the 3D reconstruction. Therefore, the mirror geometry must be considered in the correlation process. The triangulation technique is used to compute the 3D location of each point as the intersection of two rays passing through two matches in the mirrors.

## 1.4 Structured light projection in stereo vision systems

The conventional stereo vision system is composed of a single camera placed at different positions or of several cameras looking at the measuring scene. The position of a scene point with respect to one of the camera frames can be computed from its images. From the projection of a scene point in the first image, it is hard to determine its projection in the second one, but it is known according to the epipolar constraint to lie on the epipolar line corresponding to its first projection. The correspondence problem in which the relation between these projections is solved remains an interesting problem in stereo vision.

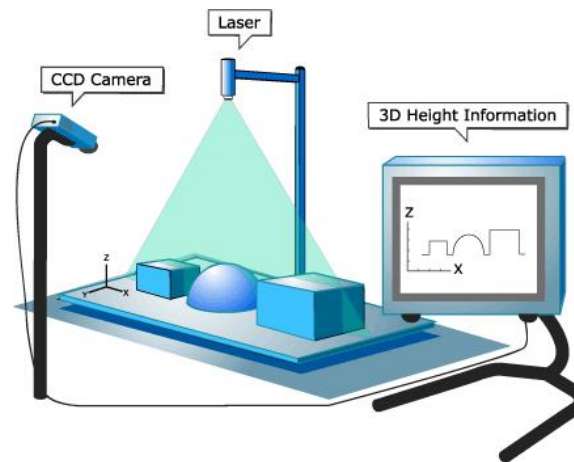


Figure 1.12: Stereo vision by structured light projection. Retrieved from [http://www.stockeryale.com/i/lasers/structured\\_light.htm](http://www.stockeryale.com/i/lasers/structured_light.htm)

The correspondence problem can be simplified using structured light system in which the second stereo camera is replaced by a structured light projector as shown in figure 1.12. From the deformation of the imaged pattern compared to the projected one, the 3D information can be achieved. In this method, the correspondences between the imaged and the emitted patterns can be found by codifying the projected pattern, i.e. adding information to the projected light. Each of the 3D points can be calculated by triangulation from the image points in the captured image and the projected one. Of course the calibration must be done before the scene point

computation. Batlle and others have conducted a complete survey on the structured light techniques used to solve the correspondence problem [Batlle et al, 1998].

## 1.5 Structured light-based catadioptric stereo sensors

Devices projecting light patterns can be slide projectors, digital projectors or laser projectors. The disadvantage of slide projectors is that the working temperature of the projector lamp causing deformations makes it hard to be used with calibrated system. Besides, the focusing problem of the digital projectors limits the depth range of the surroundings to be measured. In addition, the fact that laser light is monochromatic permits optical filters to be used for image segmentation. Lastly, such intense light like laser enhances the matching and laser projectors can be easily coupled in a compact device. For the advantages above, laser light could be a good choice for the structured light based stereo systems [Orghidan et al, 2003].



Figure 1.13: Structured light-based catadioptric stereo sensor proposed in [Orghidan et al, 2006]

Orghidan and others [Orghidan, 2006] have developed a stereo vision system using a catadioptric camera and applying the laser based structured light technique as demonstrated in figure 1.13. The proposed sensor has the coaxial configuration similar to the paracatadioptric stereo system created by Gluckman [Gluckman et al, 1998] but the lower catadioptric sensor is replaced by an omnidirectional laser projector. The laser source emits a cone of light to a conic

mirror so that the omnidirectional reflected light covers the complete view of the camera. The stereo is computed through three main steps: first the proposed sensor (composed of camera and laser projector) is modeled and calibrated, then the laser stripe is detected in the captured catadioptric image by image segmentation and finally the range scan is achieved from the detected laser profile and the sensor model.

In the Icare project, the researchers at INRIA, France have embedded to the mobile robot, namely ANIS, a vision system combining a catadioptric camera and a laser range finder to assist the robot in localization, navigation and mapping (see figure 1.14). The advantage of using a catadioptric camera together with a laser range finder is that the locations of the laser points projected into the surroundings are known with respect to the laser range finder. This additional information simplifies the calibration stage.



Figure 1.14: ANIS robot in Icare project at INRIA. Retrieved from <http://ralyx.inria.fr/2006/Raweb/icare/uid0.html>

## 1.6 Objectives

This thesis is carried out at MIS Laboratory, Amiens in order to obtain the Erasmus Mundus Master degree in Computer Vision and RoBOTics (VIBOT). The overall objective is to study and improve the calibration of the catadioptric stereo sensor. Since this work is based on the

real prototype already developed in the laboratory, the first goal is to review the calibration, measurement and application that have been accomplished for this prototype. The second goal is to develop a novel calibration method which simplifies the previous one and enhances the subsequent scene reconstruction. The performance of the proposed method will be evaluated by simulation. Once the new approach is validated with the synthetic data, the third goal is to apply this method to the omnidirectional stereo sensor. And the final goal is to use the calibrated system for scene reconstruction.

## 1.7 Thesis outline

This thesis investigates the catadioptric stereo sensor based on structured light projection and proposes a novel calibration method that allows a simpler and more efficient calibration for the sensor than the earlier one. The first chapter provides an introduction of the omnidirectional vision devices, the panoramic stereo sensors and the structured light-based catadioptric stereo sensors. The second chapter defines the problem to be solved in this thesis. The third chapter studies the sequential calibration method that has been developed for the sensor in use. The novel method, namely simultaneous calibration, is described in detail in chapter 4. Chapter 5 illustrates the results of the calibration approaches. The thesis is finished with a conclusion in chapter 6.

## Chapter 2

# Problem Definition

After designing an omnidirectional stereo sensor composed of a catadioptric camera and an omnidirectional laser projector as illustrated in figure 1.13, Orghidan and others have proposed a calibration method to estimate the parameters of each component of the sensor. In this thesis, the developed calibration is namely sequential method as it consists of two stages: first the camera is calibrated to find the intrinsic and extrinsic parameters. These parameters build up the camera model which relates each 3D point in space and its pixel point in the image plane. Then, the laser projection is calibrated to obtain the parameters of a surface that represents the laser pattern projected to the scene.

Obviously, the laser projection can not be carried out without the camera calibration as it requires the camera model resulted from the camera calibration. This is the first limitation of the sequential approach. In the camera calibration, the parameters are solved by a non-linear iterative approach using a set of 3D points on the calibration planes and their projections in the image plane. Therefore, the calibration is restricted to the use of calibration planes. Moreover, an accurate measurement of the 3D points is indispensable for a reliable calibration. Again, in the calibration of the laser projection, the calibration planes are employed to compute the 3D location of the laser points from their image points. In conclusion, the sequential calibration is complicated by the construction of the calibration planes and its accuracy depends on the measurement of these planes.

In order to improve any system or any process, it is necessary to understand the related objects in detail. Hence, the thesis firstly deals with a thorough study on the sequential calibration in order to discover possible solutions to overcome its limitation. This first task will be completed by a state of the art in chapter 3. A novel approach can be investigated to allow a simultaneous calibration for both catadioptric camera and laser projection. Furthermore, it should avoid the dependence on the use of the calibration planes or the required measurement

of the 3D points. This avoidance permits a more robust calibration method. Moreover, a comparison of the sequential method and a novel one should be performed to evaluate the possible improvement. These problems will be solved in chapter 4.

A practical way to study the performance of an approach is to use simulation. The sequential method and the novel one are simulated and compared to each other by MATLAB. The simulation results are demonstrated in chapter 5.

The dissertation is concluded by chapter 6 in which an overall comparison of the calibrations and the future works derived from the results of this thesis are presented.

## Chapter 3

# State of the Art: Sequential Calibration

This chapter firstly describes the possible arrangements of an omnidirectional camera and an omnidirectional laser projector to obtain a structured light-based omnidirectional stereo sensor. Then, the calibration that has been developed for the most suitable configuration is presented in detail.

### 3.1 Arrangements of a structured light-based catadioptric stereo sensor

A conventional structured light-based stereo sensor is formed by a perspective camera and a structured light projector to compute depth of the surrounding scene. The structured light source emits light patterns to the scene such that they cover as much as possible the camera view. In case the camera in use is catadioptric, the traditional structured-light projector is ineffective as the projected patterns are not spread over the omnidirectional field of view of the camera. Orghidan and others [Orghidan et al, 2005] have proposed the use of an omnidirectional laser projector which has a wide field of view in the same way of the catadioptric camera.

As mentioned in the introduction, an omnidirectional sensor composed of a hyperbolic mirror and a perspective camera or of a parabolic mirror and an orthographic camera fulfils the single viewpoint constraint. However, in the first configuration, it is difficult to place the camera exactly at the second focus of the hyperboloid; the hyper-catadioptric sensors are thus limited in the market and usually expensive. On the contrary, the second configuration is notably practical as the parabolic mirror and the orthographic camera can be translated arbitrarily from

each others along their coincided axes whilst holding the single viewpoint.

The omnidirectional laser projector is constructed by a laser source that emits a circle of laser to a mirror so that the reflected light spreads out the entire field of view of the camera. The mirror in use should preserve the brightness of the projected laser and does not require a single viewpoint. It has been indicated that the conical mirror is the best choice as it produces much better resolution [Yagi, 1999] and preserves the image point brightness better than the other mirrors [Lin and Bajcsy, 2001].

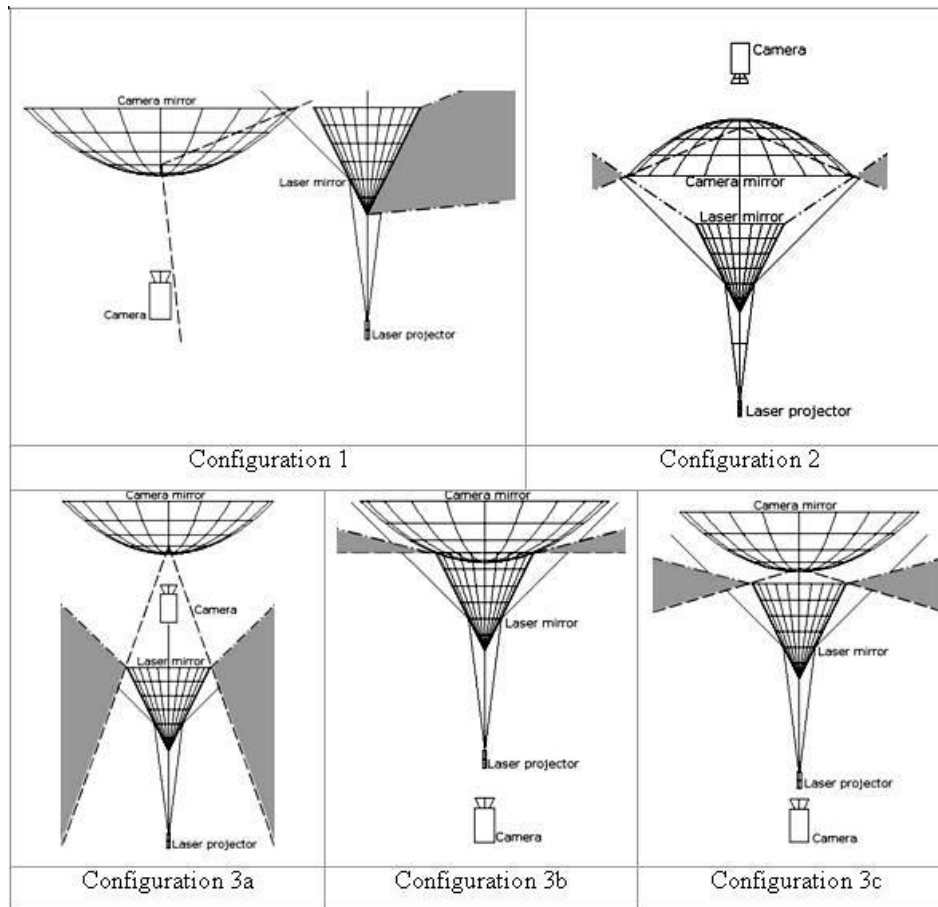


Figure 3.1: Arrangements of a catadioptric camera and an omnidirectional laser projector

Several arrangements of a catadioptric camera and an omnidirectional laser projector have been analysed in [Orghidan, 2006]. These configurations are presented in following section and illustrated in figure 3.1. The mirrors used together with the camera and the laser projector are

namely camera mirror and laser mirror respectively.

In the first configuration, the catadioptric camera and the laser projector are placed horizontally along the baseline. The laser emitted from the source is reflected by the laser mirror to the scene and the camera captures the projection of the scene onto the camera mirror. The disadvantage of this configuration is the scene occlusion caused by the laser projector in the camera field of view. In addition, part of the laser projection is hidden by the laser mirror or reflected by the camera mirror. This drawback can be overcome by placing back-to-back two mirrors of the stereo sensor as shown in the second configuration. This arrangement avoids the scene occlusion in configuration 1. However, the laser pattern must be projected out of the periphery of the parabolic mirror so that it can be imaged by the camera. Therefore, the common field of view of the laser and the camera is obviously limited. Another solution is to arrange two mirrors along a vertical translation from each others as in configuration 3a; and in that case the laser can be projected freely into the laser mirror. In order to have a more compact sensor, the omnidirectional laser projector can be placed between the camera and its mirror as presented in configurations 3b and 3c. However, this setting provides a very small amount of the stereo information. Considering all of the analyses, configuration 3a is the most suitable choice for the stereo computation. The following section reviews the modelling and calibration of this configuration.

## 3.2 Sequential calibration of structured light-based catadioptric stereo sensor

The sensor calibration is called sequential calibration as it consists of two stages: calibration of the catadioptric camera and afterwards that of the omnidirectional laser projector.

### 3.2.1 Catadioptric camera calibration using equivalent projection of a sphere

Every central catadioptric projection is equivalent to a central projection of the scene point to a sphere followed by a perspective projection from a point on an axis of the sphere to a plan perpendicular to that axis [Geyer and Daniilidis, 2000]. Orghidan has used this projective equivalence to model and calibrate the catadioptric camera using parabolic mirror [Orghidan, 2006]. Considering the world point  $P_W(x_W, y_W, z_W)$ , its central projection to a sphere of radius  $R$  centred at the focus of the paraboloid is  $P_S(x_S, y_S, z_S)$ . Then the formation of the image point  $P_i(x, y)$  is completed by the perspective projection of  $P_S$  from  $C(0, 0, \xi)$  to the image plan

as illustrated in figure 3.2.

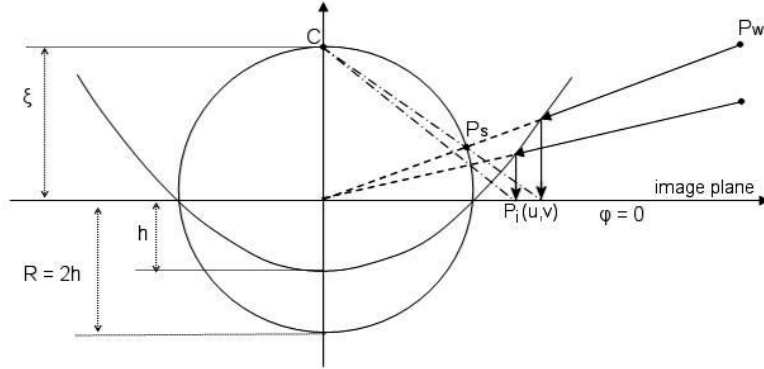


Figure 3.2: Image formation using the projective equivalence of a central catadioptric

The relation between the world point  $P_W$  and its central projection  $P_S$  onto the sphere is given by equation (3.1).

$$\begin{cases} x_S = \lambda x_W \\ y_S = \lambda y_W \\ z_S = \lambda z_W \end{cases} \quad (3.1)$$

Since  $P_S$  belongs to the sphere, its coordinates satisfy equation (3.2).

$$x_S^2 + y_S^2 + z_S^2 = R^2 \quad (3.2)$$

The perspective projection of  $P_S$  from  $C(0, 0, \xi)$  to the image plan at distance  $\varphi$  from the sphere centre produces the image point  $P_i(x, y)$  satisfying equation (3.3).

$$\begin{cases} \frac{x_S}{\xi - z_S} = \frac{x}{\xi + \varphi} \\ \frac{y_S}{\xi - z_S} = \frac{y}{\xi + \varphi} \end{cases} \quad (3.3)$$

Applying the transformation from the image point to the pixel point using the camera intrinsic parameters  $(\alpha_u, \alpha_v, u_0, v_0)$ , the unified model of the catadioptric camera is expressed in equation (3.4).

$$\begin{cases} u = \alpha_u \frac{(\xi + \varphi)x_W}{\xi \sqrt{x_W^2 + y_W^2 + z_W^2} - z_W} + u_0 \\ v = \alpha_v \frac{(\xi + \varphi)y_W}{\xi \sqrt{x_W^2 + y_W^2 + z_W^2} - z_W} + v_0 \end{cases} \quad (3.4)$$

The catadioptric camera is calibrated using a set of known 3D points  $P_W$  distributed on four calibration planes enclosing the sensor and the corresponding pixel points  $(u, v)$  extracted in the omnidirectional image.

The calibration parameters are as follows:

- $\xi$  depending on the eccentricity,  $\varphi$  depending on the eccentricity and the scale,
- $\alpha_u, \alpha_v, u_0, v_0$ : intrinsic camera parameters,
- $\alpha, \beta, \gamma, t_X, t_Y, t_Z$ : extrinsic camera parameters describing of the orientation and translation of the camera with respect to the world.

From the 3D points, the pixel points are calculated using the unified model. The distance between the computed pixels and those being detected in the captured image is minimized by a non-linear iterative algorithm such as Levenberg-Marquardt. The model parameters are estimated after the minimization.

The choice of the calibration patterns on which are distributed the 3D points is an important aspect as it decides the accuracy of the 3D point information and ultimately a reliable calibration. Many calibration patterns have been experimented in [Orghidan, 2006] such as grid, dot and checker patterns as shown in figure 3.3, and the checker one has shown the best performance.

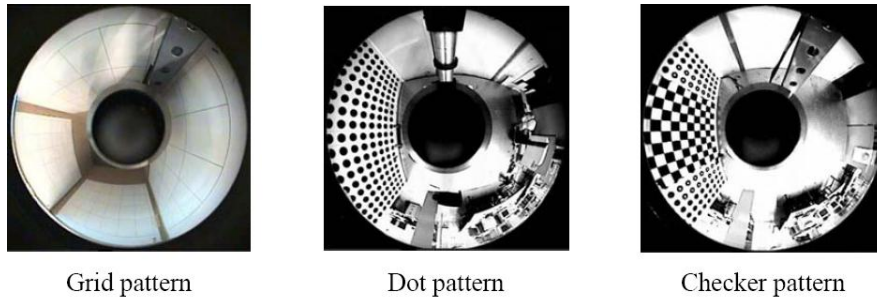


Figure 3.3: Calibration patterns experimented in [Orghidan, 2006]

### 3.2.2 Omnidirectional laser projector calibration

The omnidirectional laser projector is composed of a laser source that emits a laser circle to a conical mirror. If the laser emitter and the conical mirror are perfectly aligned, the laser reflected by the mirror spreads out the surroundings as a cone of optical rays as shown in figure 3.4 (left). These optical rays intersect with known calibration planes forming a set of 3D points which can be captured by the catadioptric camera (see figure 3.5). The locations of these 3D laser points can be computed from their 2D projections in the image and the camera parameters obtained from the first stage of the sensor calibration. In other words, the 2D points are back-projected to the points on the sphere using camera parameters estimated in the previous stage.

The intersections of the optical rays passing through those points on the sphere and the known calibration planes determine the 3D laser points. Then, a quadratic surface is fitted to these points to present a parameterised model of the laser projection.

The equation of a 3D quadratic surface can be expressed by (3.5). The intersections of this surface with the calibration planes perpendicular to X-axis and Y-axis are presented in equations (3.6) and (3.7) respectively.

$$\begin{bmatrix} x & y & z \end{bmatrix} \cdot \begin{bmatrix} a_{11} & a_{12} & a_{13} \\ a_{21} & a_{22} & a_{23} \\ a_{31} & a_{32} & a_{33} \end{bmatrix} \cdot \begin{bmatrix} x \\ y \\ z \end{bmatrix} + \begin{bmatrix} x & y & z \end{bmatrix} \cdot \begin{bmatrix} \beta_1 \\ \beta_2 \\ \beta_3 \end{bmatrix} + f = 0 \quad (3.5)$$

$$\begin{bmatrix} y & z \end{bmatrix} \cdot \begin{bmatrix} a_{22} & a_{23} \\ a_{32} & a_{33} \end{bmatrix} \cdot \begin{bmatrix} y \\ z \end{bmatrix} + \begin{bmatrix} y & z \end{bmatrix} \cdot \begin{bmatrix} P_x \\ Q_x \end{bmatrix} + R_x = 0 \quad (3.6)$$

$$\begin{bmatrix} x & z \end{bmatrix} \cdot \begin{bmatrix} a_{11} & a_{13} \\ a_{31} & a_{33} \end{bmatrix} \cdot \begin{bmatrix} x \\ z \end{bmatrix} + \begin{bmatrix} x & z \end{bmatrix} \cdot \begin{bmatrix} P_y \\ Q_y \end{bmatrix} + R_y = 0 \quad (3.7)$$

Therefore, the equations of the arcs on each calibration plane can be obtained by fitting the corresponding points to equations (3.6) and (3.7). Most of the parameters of the quadratic surface are estimated from these two equations. The others,  $a_{12}$  and  $a_{21}$ , correspond to the elliptical crossing of the quadratic and the horizontal plane.

In general, the laser projection has the shape of a cone. If there is a special configuration between the aperture angle of the conical mirror and the fan angle of the emitted laser cone, the projected pattern becomes a plane as illustrated in figure 3.4 (right). And in that case, the intersections of the laser plane and the calibration planes are straight lines which are imaged to elliptical arcs in the catadioptric image as illustrated in figure 3.6. The prototype used by Orghidan in [Orghidan, 2006] satisfies this particular configuration. Therefore, the laser projection is parameterised by a plane described in equation (3.8).

$$ax + by + cz + d = 0 \quad (3.8)$$

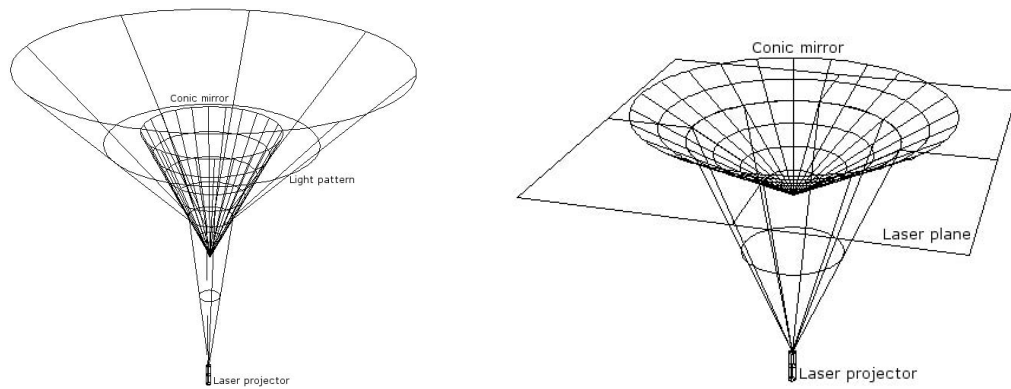


Figure 3.4: Omnidirectional projection of a structured light

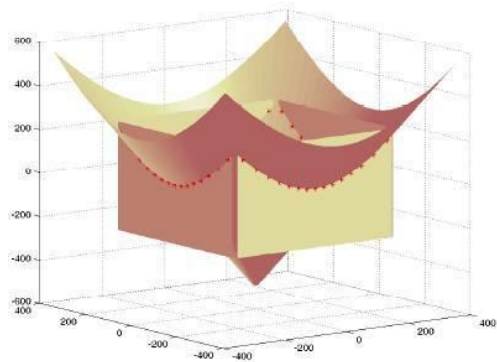


Figure 3.5: Intersections of the cone of laser projection with calibration planes

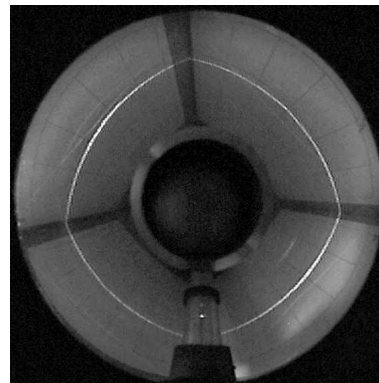


Figure 3.6: Laser strips are straight lines on the calibration planes and elliptical arcs in image if the laser projection is plan



## Chapter 4

# Novel Approach: Simultaneous Calibration

The structured light-based catadioptric stereo sensor is constructed by a catadioptric camera and an omnidirectional laser projector. Previously, the camera and the laser projector are calibrated sequentially to estimate the parameters of the system. This thesis proposes a novel calibration which permits a simultaneous calibration for both components. The actual chapter starts with the sensor modelling based on the unified model of the camera and the geometry of the laser ray. The model of the sensor is then exploited to calibrate the catadioptric camera and the omnidirectional laser projection concurrently. The proposed method is experimented and compared with the sequential calibration by simulations.

### 4.1 Sensor modelling

In the sequential calibration proposed in [Orghidan, 2006], the camera is first calibrated using a set of 3D points distributed on the known patterns placed around the sensor and their 2D projections in the image plane. To calibrate the omnidirectional structured light projection, the laser is projected on four identified planes enclosing the sensor. The locations of the laser spots on these planes are calculated from their 2D images and the camera model obtained from the camera calibration. Afterwards, the laser projection is modelled by fitting a parameterised surface to the laser spots.

The previous two-stage calibration can be simplified by a unified calibration or, in other words, a simultaneous calibration for both the camera and the laser projection using a set of laser points in 3D space and their images captured by the camera, which means that only a

single omnidirectional image containing the laser spots is necessary.

The simultaneous calibration requires a complete model that relates the 3D laser points and their image points through the parameters of the camera and the laser projection. This complete model is presented in the following sections.

The sphere of equivalent model in the previous chapter is employed again to describe the relation of the laser points projected onto the scene and the corresponding pixels in the image plane through the camera parameters.

Considering the laser point  $P_W(x_W, y_W, z_W)$  with respected to the camera coordinate system  $\{C : x_C, y_C, z_C\}$  centred at the focus of the parabolic mirror (or the centre of the sphere), its pixel coordinates  $(u, v)$  are calculated by equation (4.1) using the sensor parameters depending on the shape of the mirror  $(\xi, \varphi)$  and the intrinsic parameters of the camera  $(\alpha_u, \alpha_v, u_0, v_0)$ .

$$\begin{cases} u = \alpha_u \frac{(\xi + \varphi)x_W}{\xi \sqrt{x_W^2 + y_W^2 + z_W^2 - z_W}} + u_0 \\ v = \alpha_v \frac{(\xi + \varphi)y_W}{\xi \sqrt{x_W^2 + y_W^2 + z_W^2 - z_W}} + v_0 \end{cases} \quad (4.1)$$

Moreover, the laser point also belongs to the optical ray in the cone of laser reflected by the conical mirror as shown in figure 4.1. This fact can be exploited to describe the connection of the 3D and 2D points through the parameters of the laser projection.

Supposing that the laser emitter and the conical mirror are perfectly aligned, the 3D shape of the reflected laser pattern is a vertical circular cone. The apex of this cone is chosen as the origin of the laser coordinate system  $\{L : x_L, y_L, z_L\}$  as illustrated in figure 4.1. To simplify the problem, let  $\{L\}$  be the translation of  $\{C\}$  along the Z-axis with a distance  $h$ , therefore the location of  $\{L\}$  with respected to  $\{C\}$  is  $(0, 0, -h)^T$ . And there is no rotation between  $\{C\}$  and  $\{L\}$ . The baseline between the camera and the laser coordinate systems is vertical.

Considering a laser ray passing through the 3D point  $P_W(x_W, y_W, z_W)$  (note that the coordinates  $(x_W, y_W, z_W)$  are measured in  $\{C\}$ ), the azimuth angle and the tilt angle of this ray in the laser coordinate system  $\{L\}$  are  $\alpha$  and  $\beta$  respectively as shown in figure 4.2. This optical beam can be expressed in  $\{L\}$  by equations (4.2).

$$\begin{cases} x_W = (z_W + h) \cdot \tan \beta \cdot \cos \alpha \\ y_W = (z_W + h) \cdot \tan \beta \cdot \sin \alpha \end{cases} \quad (4.2)$$

In equations (4.2),  $h$  and  $\beta$  are the parameters representing the cone of laser projection.  $h$  depends on the position of the laser-conical mirror set with respected to  $\{C\}$ .  $\beta$  depends on the fan angle of the laser emitted from the source and the open angle of the laser mirror (conical one). The azimuth angle  $\alpha$  of any laser ray is also the angle between the vertical plane containing that ray and the vertical plane containing the X-axes of all coordinate systems. Therefore, the angle  $\alpha$  can be computed in the image plane by equation (4.3).

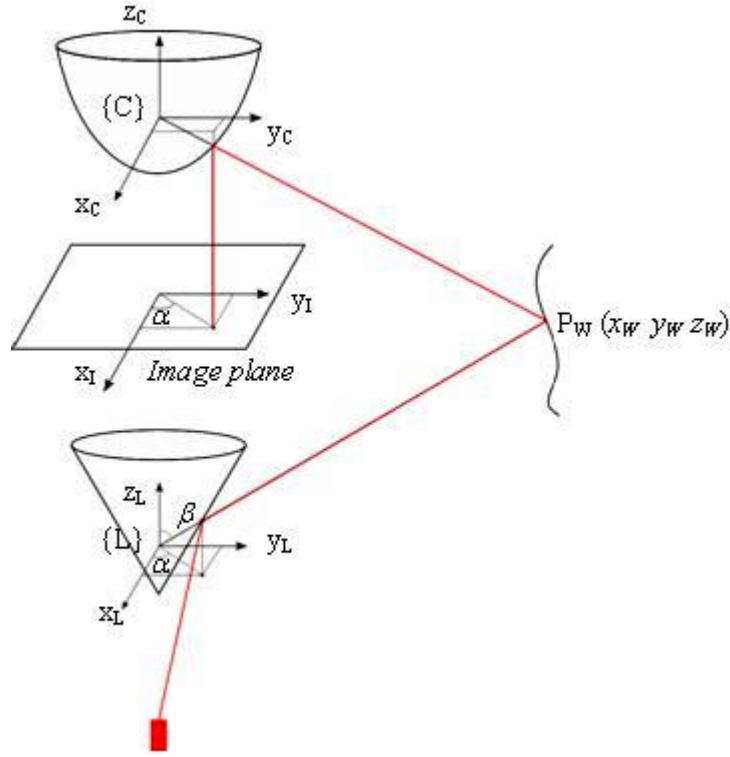


Figure 4.1: Triangulation of the laser point in 3D space, the camera and the laser projection coordinate systems

$$\begin{cases} \cos\alpha = \frac{x_I}{\sqrt{x_I^2 + y_I^2}} \\ \sin\alpha = \frac{y_I}{\sqrt{x_I^2 + y_I^2}} \end{cases} \quad (4.3)$$

where  $(x_I, y_I)$  can be calculated from the pixel coordinates as follows:

$$\begin{cases} x_I = \frac{u - u_0}{\alpha_u} \\ y_I = \frac{v - v_0}{\alpha_v} \end{cases} \quad (4.4)$$

From equations (4.2), (4.3) and (4.4), the next ones are obtained:

$$\begin{cases} x_W = (z_W + h) \cdot \tan\beta \cdot \frac{(u - u_0)}{\alpha_u} / \sqrt{\left(\frac{u - u_0}{\alpha_u}\right)^2 + \left(\frac{v - v_0}{\alpha_v}\right)^2} \\ y_W = (z_W + h) \cdot \tan\beta \cdot \frac{(v - v_0)}{\alpha_v} / \sqrt{\left(\frac{u - u_0}{\alpha_u}\right)^2 + \left(\frac{v - v_0}{\alpha_v}\right)^2} \end{cases} \quad (4.5)$$

The above equations relate the 3D laser points and the pixel points by the intrinsic param-

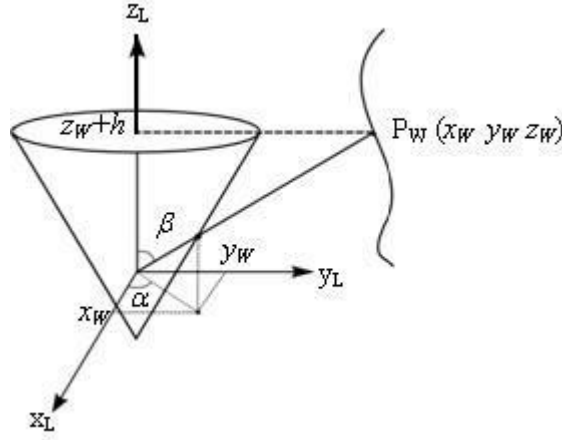


Figure 4.2: Geometry of an optical ray in the cone of projected laser pattern

eters of the camera and the parameters of the laser projection. Finally, the complete model of the structured light-based catadioptric stereo sensor is given by:

$$\begin{cases} u = \alpha_u \frac{(\xi + \varphi)x_W}{\xi \sqrt{x_W^2 + y_W^2 + z_W^2 - z_W}} + u_0 \\ v = \alpha_v \frac{(\xi + \varphi)y_W}{\xi \sqrt{x_W^2 + y_W^2 + z_W^2 - z_W}} + v_0 \\ x_W = (z_W + h) \cdot \tan \beta \cdot \left( \frac{u - u_0}{\alpha_u} \right) / \sqrt{\left( \frac{u - u_0}{\alpha_u} \right)^2 + \left( \frac{v - v_0}{\alpha_v} \right)^2} \\ y_W = (z_W + h) \cdot \tan \beta \cdot \left( \frac{v - v_0}{\alpha_v} \right) / \sqrt{\left( \frac{u - u_0}{\alpha_u} \right)^2 + \left( \frac{v - v_0}{\alpha_v} \right)^2} \end{cases} \quad (4.6)$$

This complete model allows the parameters of the camera and the laser projection to be solved using a set of 3D points  $(x_W, y_W, z_W)$  and 2D points  $(u, v)$ . These parameters are listed below:

- The parameters of the parabolic mirror used with the camera:  $\xi, \varphi$
- The intrinsic parameters of the camera:  $\alpha_u, \alpha_v, u_0, v_0$
- The parameters of the cone of laser projection:  $h, \beta$  ( $h$  represents the position of the cone of laser with respect to  $\{C\}$ .  $\beta$  depends on the fan angle of the laser emitted from the projector and the open angle of the laser conical mirror)

## 4.2 Simultaneous calibration

All the calculation in this work is done in  $\{C\}$  coordinate system; hence the extrinsic parameters relating the world coordinate system and the camera coordinate system are not considered. The

baseline of the whole system coincides with the symmetrical axis of the paraboloidal mirror, the camera, the conical mirror and the laser projector. There is no rotation between  $\{C\}$  and  $\{L\}$ .

The non-linear equations in (4.6) relate the laser points in the scene  $P_W(x_W, y_W, z_W)$  and the pixel points  $(u, v)$  through the parameters of the sensor as follows:

- The parameters of the camera mirror:  $\xi, \varphi$
- The intrinsic parameters of the camera:  $\alpha_u, \alpha_v, u_0, v_0$
- The parameters of the cone of laser pattern:  $h, \beta$

These parameters can be estimated from a set of 3D points and their corresponding 2D projections by a non-linear iterative algorithm such as Levenberg Marquardt.

An interesting remark is that there are four equations in (4.6) for each laser point in 3D space; hence  $4N$  equations for  $N$  points. If the locations of these laser points  $(x_W, y_W, z_W)$  are also unknowns, there are  $3N+8$  unknowns. As the number of equations is superior to the number of unknowns, it is possible to estimate eight parameters defined above and the locations of 3D points with a sufficient number of equations. However, a system of non-linear equations may have different solutions, and in that case more constraints are necessary to obtain the correct solution.

### 4.3 Comparison of the sequential and simultaneous calibrations

The sequential calibration proposed in [Orghidan, 2006] and the simultaneous calibration in this thesis will be evaluated under simulation.

Firstly, the parameters of the sensor  $(\xi, \varphi, \alpha_u, \alpha_v, u_0, v_0, h, \beta)$  are generated as follows:

- The mirror is parabolic:  $\xi = 1$  and  $\varphi = 0$
- The intrinsic parameters of the camera:  $\alpha_u = 55, \alpha_v = -55, u_0 = 400$  and  $v_0 = 300$
- The cone of laser projection:  $h = 200$  and  $\beta = \frac{\pi}{3}$

The synthetic 3D points are created representing the intersections of the cone of laser pattern and several walls placed around the sensor as shown in figure 4.3a. These 3D points are perturbed with Gaussian noise. Then, the pixel points are computed from the synthetic 3D points and the parameters of the sensor using the camera model in equation (4.1). Gaussian noise is also added to the pixel points to obtain the noisy 2D points as illustrated in figure 4.3b.

These set synthetic points are used for both calibration methods to evaluate and compare their performance.

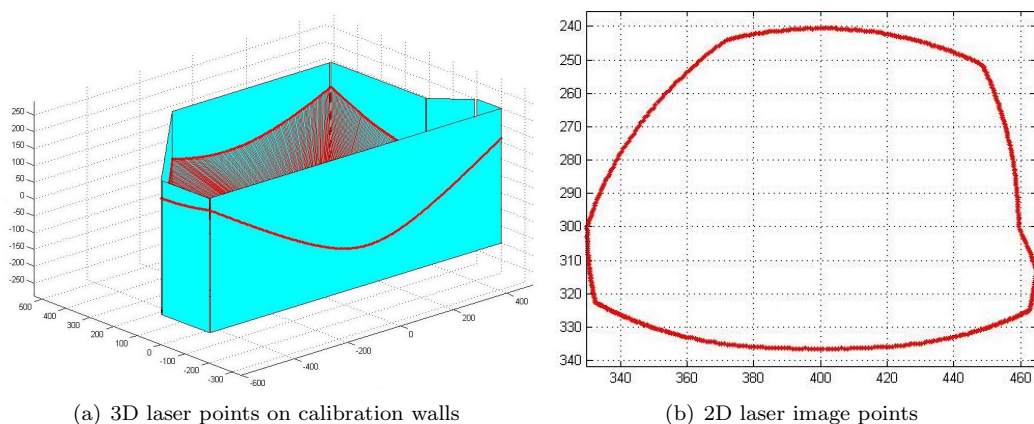


Figure 4.3: Synthetic laser points

### 4.3.1 Sequential calibration

The sequential calibration proposed in [Orghidan, 2006] is composed of two stages:

- The first stage is to calibrate the catadioptric camera. The parameters of the camera  $(\xi, \varphi, \alpha_u, \alpha_v, u_0, v_0)$  are estimated from the noisy 3D points and 2D points created in the simulation by a non-linear iterative algorithm such as Levenberg Marquardt.
- The second stage is to calibrate the cone of projected laser pattern. Given an omnidirectional image containing the laser stripes, the 3D laser intersections on the calibration planes must be reconstructed and fitted to a surface that represents the cone of laser pattern.

The non linear system in the first stage can be solved by the Least square non linear function supported by MATLAB.

The simulation for the second stage is presented in detail in the next sections:

#### **Step 1: From pixel points to points on sphere**

Given a pixel point  $(u, v)$ , the same point in metric  $P_I(x_I, y_I)$  in the image plane with respected to the camera coordinate system is expressed in equation (4.7).

$$\begin{cases} x_I = \frac{u-u_0}{\alpha_u} \\ y_I = \frac{v-v_0}{\alpha_v} \end{cases} \quad (4.7)$$

The back-projection of  $P_I$  onto the sphere of equivalence, namely  $P_S$ , can be calculated by equation (4.8).

$$\begin{cases} x_S = \frac{\xi - z_S}{\xi + \varphi} \cdot x_I \\ y_S = \frac{\xi - z_S}{\xi + \varphi} \cdot y_I \\ z_S = \frac{-k_1 - \sqrt{k_1^2 - 4k_0k_2}}{2k_2} \end{cases} \quad (4.8)$$

where

$$\begin{cases} k_0 = \xi^2(x_I^2 + y_I^2) - (\xi + \varphi)^2 \\ k_1 = -2\xi(x_I^2 + y_I^2) \\ k_2 = (x_I^2 + y_I^2) + (\xi + \varphi)^2 \end{cases} \quad (4.9)$$

**Step 2: From points on sphere to laser points on calibration planes and fit a cone to these laser points**

The 3D laser spots on the calibration planes are computed by intersections of the rays passing through the points on the sphere and those planes. The laser spot on the calibration plane belongs to the ray passing through the centre of the sphere and the point on the sphere ; therefore its coordinates are given by:

$$\begin{bmatrix} x_P \\ y_P \\ z_P \end{bmatrix} = t \cdot \begin{bmatrix} x_S \\ y_S \\ z_S \end{bmatrix} \quad (4.10)$$

where t is unknown.

Projecting this point to the calibration plane defined by equation (4.11), the location of the laser spot can be computed by (4.12).

$$Ax + By + Cz + D = 0 \quad (4.11)$$

$$\begin{bmatrix} x_P \\ y_P \\ z_P \end{bmatrix} = \frac{-D}{Ax_S + By_S + Cz_S} \cdot \begin{bmatrix} x_S \\ y_S \\ z_S \end{bmatrix} \quad (4.12)$$

A circular cone is fitted to these laser points on the calibration planes. The parameters of the fitted cone, i.e. the vertex, the aperture angle and the direction, represent the model of the laser projection.

**Step 3: Reconstruction of 3D points**

The 3D points are reconstructed by triangulation of the rays passing through the points

on the sphere computed in equations (4.8) and the laser rays belonging to the estimated laser cone. The intersection of a ray passing through the point on the sphere and the laser cone is presented below.

The 3D point  $X(x_W, y_W, z_W)$  lies on the ray passing through the centre of the sphere  $(0, 0, 0)$  and the point  $(x_S, y_S, z_S)$  on the sphere; hence its coordinates are given by:

$$\begin{bmatrix} x_W \\ y_W \\ z_W \end{bmatrix} = t \cdot \begin{bmatrix} x_S \\ y_S \\ z_S \end{bmatrix} \quad (4.13)$$

Note that  $x_P$  in (4.10) is used for cone fitting in step 2 and  $x_W$  in (4.13) is used for reconstruction in step 3 and they are computed from different images: image for calibration and image for reconstruction respectively. The 3D point also belongs to the cone of laser; therefore it satisfies:

$$\begin{cases} (X - V)^T M (X - V) = 0 \\ A(X - V) \geq 0 \\ M = A \cdot A^T - (\cos\theta)^2 I \end{cases} \quad (4.14)$$

where  $A$ ,  $\theta$  and  $V$  are respectively the direction, the slope and the vertex of the cone. Replacing (4.13) in (4.14) and simplifying the resulted equation, we obtained:

$$c_2 t^2 + 2c_1 t + c_0 = 0 \quad (4.15)$$

in which

$$\begin{cases} c_2 = D^T M D, c_1 = D^T M S, c_0 = S^T M S \\ D = (x_S, y_S, z_S)^T \\ S = -V \end{cases} \quad (4.16)$$

The solutions of (4.15) determine the intersection of the ray and the cone as follows:

$c_2 \neq 0$ $(\delta = c_1^2 - c_0 c_2)$	$\delta < 0$ $\delta = 0$ $\delta > 0$	No intersection The ray is tangent to the cone with $t = -c_1/c_2$ Two intersections with $t = (-c_1 \pm \sqrt{\delta})/c_2$
$c_2 = 0$	$c_1 \neq 0$ $c_1 = 0$	The ray is parallel to the cone wall, one intersection with $t = -c_0/(2c_1)$ $c_0 = 0$ : The ray belongs to the cone wall

The error between those points and the synthetic 3D points created at the beginning of the simulation is computed and used as a criterion to compare two calibration methods.

### 4.3.2 Simultaneous calibration

The non-linear equations in (4.6) are used to calibrate the catadioptric camera and the laser projection simultaneously. As explained in section 4.2, with those equations, it is possible to estimate the sensor parameters and the unknown 3D points from the 2D laser points in the image plane. However, to compare with the sequential calibration, the same set of synthetic points are used to estimate the parameters. In addition, after the iterative algorithm had solve the system of non-linear equations in (4.6), a new set of 3D points is also estimated, which is the 3D reconstruction from the 2D points. The distance between those points and the synthetic 3D points are calculated and compared to the reconstruction error given by the sequential method.



# Chapter 5

## Experimental Results

### 5.1 Comparison of two calibration methods

The sequential calibration developed in [Orghidan, 2006] and the simultaneous one proposed in this thesis are implemented and compared under simulation with the procedure described in section 4.3. Each calibration method is evaluated by eight trials in which:

- Various Gaussian noises are added to the synthetic 3D points to simulate the error in the measurement of the 3D points.
- Various Gaussian noises are added to the synthetic pixel points to simulate the error in the pixel detection in images.
- Various sets of parameters are tested to verify the ability of convergence of the non-linear iterative approach.

Note that the same noises and sets of parameters are used for both methods in each trial to validate the comparison. The details of each trial are as follows.

Trials	1	2	3	4	5	6	7	8
Noise in 3D points with standard deviation of 2	X		X		X		X	
Noise in 3D points with standard deviation of 4		X		X		X		X
Noise in 2D points with standard deviation of 0.05	X	X			X	X		
Noise in 2D points with standard deviation of 0.1			X	X			X	X
Initial parameters $(\xi, \varphi, \alpha_u, \alpha_v, u_0, v_0, h, \beta)$ (1.01,0.01,55.60,-54.40,404.00,303.00,1.06,202.00)	X	X	X	X				
Initial parameters $(\xi, \varphi, \alpha_u, \alpha_v, u_0, v_0, h, \beta)$ (1.10,0.10,57.00,-53.00,410.00,310.00,1.20,210.00)					X	X	X	X

The calibration methods are also evaluated with a surrounding scene of two different ranges: small range with a dimension of about 1000mm and large range of 5000mm. The reconstruction errors of two approaches are illustrated in figures 5.1 and 5.2. There are 580 laser points in total.

The presented error is the average distance from the reconstructed 3D points and the synthetic ones generated at the beginning of the simulation.

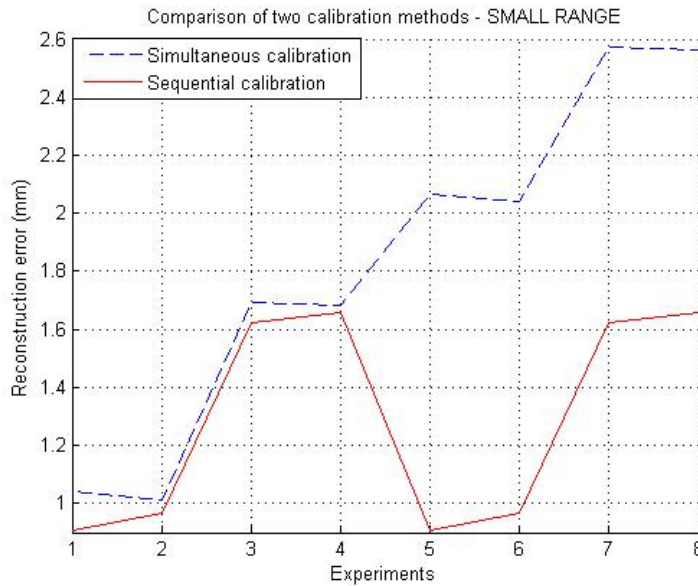


Figure 5.1: Reconstruction errors of the sequential and simultaneous calibrations with a surrounding environment of small range

It can be seen from figures 5.1 and 5.2 that the novel calibration provides slightly higher reconstruction errors than the sequential calibration if the environment is small, but better results with a large environment. The possible reason is that the sequential calibration performs well with the calibration patterns enclosing the sensor at short distances. A better accuracy with the large environment should be an advantage of the simultaneous method over the other because this novel method allows the 3D points to be reconstructed along with the calibration as mentioned in section 4.3 and the reconstruction is usually carried out with a large surrounding scene.

The complete model of the simultaneous calibration presented in equations (4.6) has shown that this method can also solve the parameters if the 3D points are not well defined as there are  $(3N+8)$  unknowns (eight parameters and  $3N$  coordinates of  $N$  points) and  $4N$  equations. However, the non-linear system in (4.6) may have different solutions, and in that case using

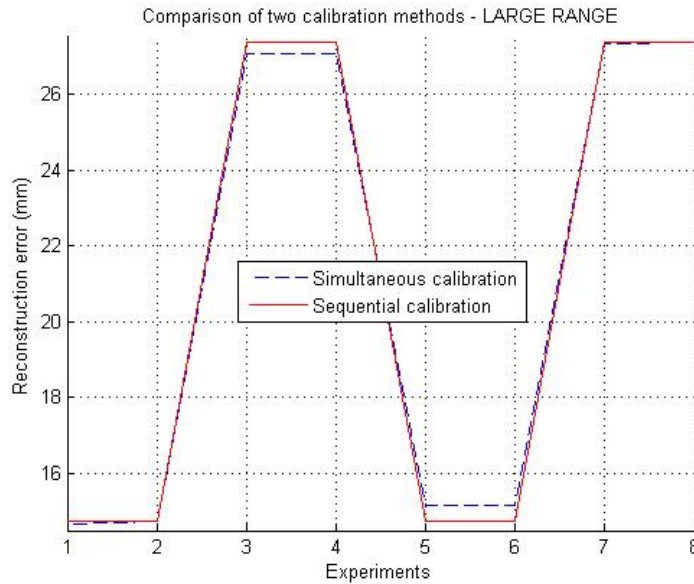


Figure 5.2: Reconstruction errors of the sequential and simultaneous calibrations with a surrounding environment of large range

only the pixel points is not sufficient to estimate the sensor parameters and the unknown 3D points; hence some constraint about the 3D points is necessary. This constraint can be an estimation about the 3D laser points as presented in the next experiment.

The two calibrations are again evaluated using a special set of 3D points. This set of 3D points is not the one created at the beginning of the simulation but has the similar structure. This means that the 3D points are not measured but they are estimated when the laser is projected to the scene. For example, the scene is structured by seven walls as illustrated in figure 4.3a, the laser spots on these walls can be estimated as follows:  $x$  and  $y$  are estimated from the locations of these walls with respect to the sensor and  $z$  is estimated from  $x, y$  and the shape of the laser cone. In other words, the coordinates of the laser points projected to the scene can be approximated by the structure of the scene.

Figures 5.3 shows the comparison result of the sequential and simultaneous calibrations with the increased error in the approximation of the 3D points. It is obviously that the simultaneous method is much better than the sequential one if the 3D points used for calibration are not accurately measured. In an environment of about 5000 mm, using a set of 3D points with an approximation error of 5%, the reconstruction error of the simultaneous approach is about 90 mm (0.18% of the scene dimension) whereas the sequential one provides an error of about 310 mm (0.62% of the scene dimension). Moreover, the error created by the sequential method

raises significantly when the uncertainty about the structure of the scene to be reconstructed increases.

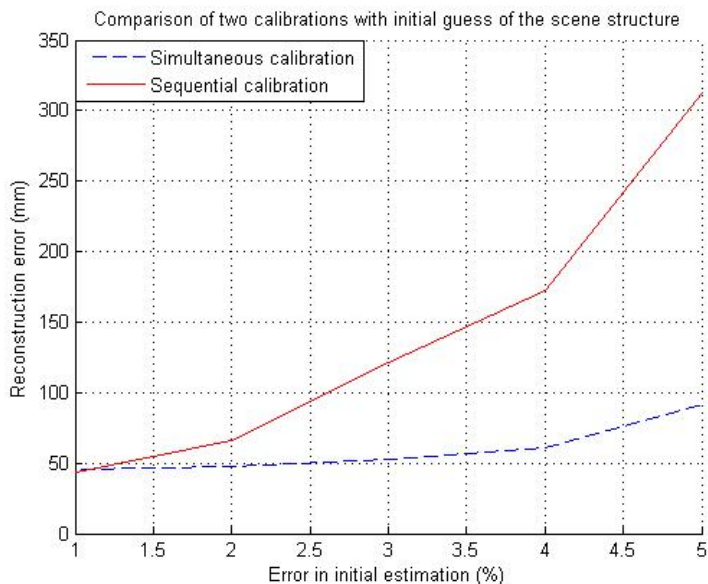


Figure 5.3: Reconstruction errors of two calibrations using 3D points approximated from the scene structure with a surrounding environment of large range

## 5.2 Combination of two calibration methods

The simultaneous calibration requires some constraint about the 3D points used to initialise the non-linear iterative algorithm. This section shows an experiment in which the estimated parameters and the 3D points reconstructed from the sequential method are used as initial values for the simultaneous one to verify whether the accuracy of the scene reconstruction can be improved by this combination or not.

The results demonstrated in figures 5.4 and 5.5 show that the simultaneous calibration does not enhance the 3D reconstruction when using the results from sequential method to initialise the non-linear iterative algorithm.

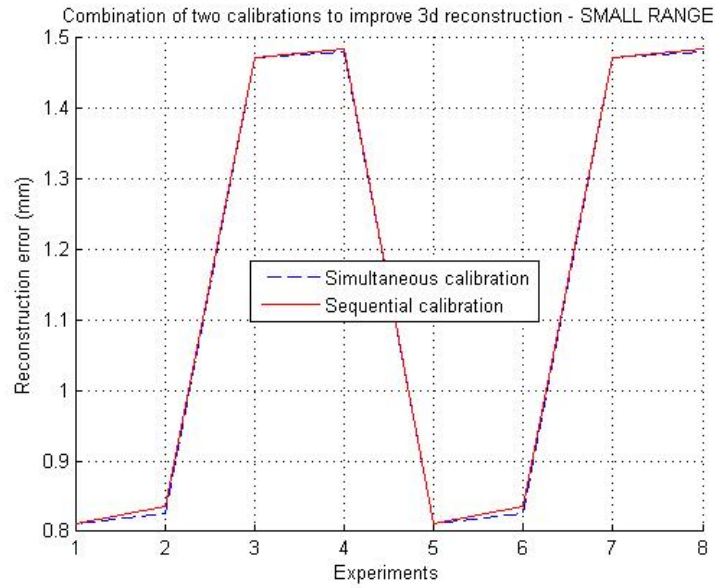


Figure 5.4: Reconstruction errors of the sequential and simultaneous calibrations when combining these two approaches with a surrounding environment of small range

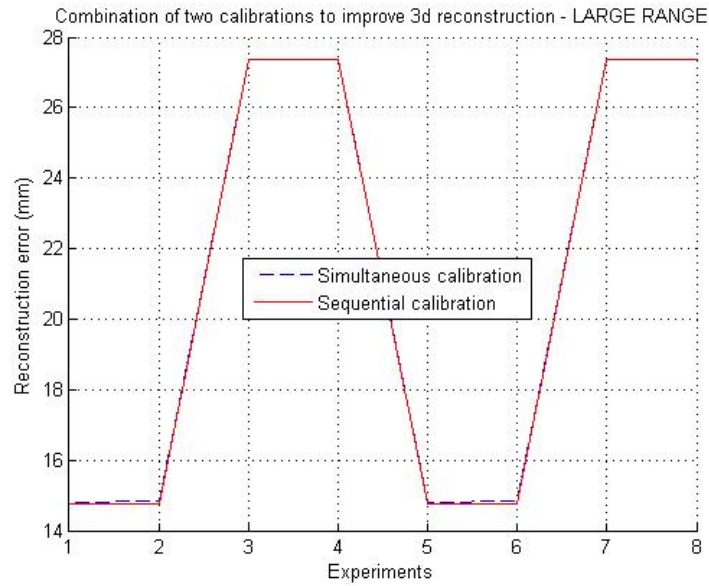


Figure 5.5: Reconstruction errors of the sequential and simultaneous calibrations when combining these two approaches with a surrounding environment of large range



# Chapter 6

## Conclusions

### 6.1 Conclusions

This thesis is focused on a novel calibration approach for the catadioptric stereo sensor based on structured light projection. This method is proved by simulation to be simpler and more robust than the calibration that has been developed for the same stereo system.

The thesis is started with a general introduction about omnidirectional vision devices with their characteristics, the omnidirectional stereo systems and lastly the laser-based catadioptric stereo sensor.

Chapter 2 describes the sequential method in which the catadioptric camera and the omnidirectional laser projector are calibrated consecutively. This method has been proposed in [Orghidan, 2006].

Chapter 3 provides the details of the novel approach that allows a simultaneous calibration for the camera and the laser projector. A complete model of the sensor is obtained by using the projection model of the camera and the geometry of the projected laser pattern. These two calibration methods are evaluated and compared by simulation with a set of synthetic 3D and 2D points. The simulation results have shown that:

- Two calibration methods provide similar reconstruction accuracy if the 3D points use for the calibration are well known.
- Concerning the sensor modelling, the sequential method uses the projection model of the camera while the simultaneous one adds to that model the representation of the laser projection. However, the laser projection is easily modelled by geometry; hence, there is no significant complexity.

- The sequential method requires the calibration patterns placed around the sensor whereas the simultaneous one does not as it can employ directly the laser profile projected to the scene. Moreover, in the sequential approach, the 3D points should be well measured to ensure a reliable calibration. This limitation is overcome by the simultaneous calibration in which the 3D laser points can be approximated from the structure of the scene.

## 6.2 Future works

In three months, this thesis has completed the development and evaluation of the novel calibration by simulation. The further step will be to validate this method with the prototype of the structured light-based catadioptric stereo sensor in the laboratory.

Once the sensor is calibrated, it can be used for further applications such as scene reconstruction, environment inspection, robot navigation, etc. Therefore, an interesting research path after this MSc thesis is to embed this stereo sensor on a mobile robot to assist this automaton in the localisation, navigation and mapping tasks.

# Bibliography

- [1] D.W. Rees. Panoramic television viewing system. In *United States Patent No. 3, 505, 465*, 1970.
- [2] Y. Yagi and S. Kawato. Panoramic scene analysis with conic projection. In *IEEE/RSJ International Conference on Intelligent Robots and Systems*, Vol. 1, pp. 181-187, 1990.
- [3] J. Hong, X. Tan, B. Pinette, R. Weiss and E.M. Riseman. Image-based homing. In *IEEE International Conference on Robotics and Automation*, pp. 620-625, vol. 1, 1991.
- [4] K. Yamazawa, Y. Yagi and M. Yachida. Omnidirectional imaging with hyperboloidal projection. In *IEEE/RSJ International Conference on Intelligent Robots and Systems*, pp. 1029-1034, 1993.
- [5] C. Pegard and E.M. Mouaddib. A mobile robot using a panoramic view. In *IEEE International Conference on Robotics and Automation*, Vol. 1, pp. 89-94, 1996.
- [6] S.K. Nayar. Catadioptric omnidirectional camera. In *IEEE International Conference on Computer Vision and Pattern Recognition*, pp. 482-488, 1997.
- [7] S.K. Nayar and S. Baker. Catadioptric image formation. In *Proceedings of DARPA Image Understanding Workshop*, pp. 1431-1437, 1997.
- [8] S. Baker and S.K. Nayar. A Theory of Single-Viewpoint Catadioptric Image Formation. In *International Journal of Computer Vision* 35(2), 175-196, 1999.
- [9] V.S. Nalwa. A true omnidirectional viewer. In Technical report, Bell Laboratories, Holmdel, NJ 07733, USA, February 1996.
- [10] Y. Yagi and M. Yachida. Real-time generation of environmental map and obstacle avoidance using omnidirectional image sensor with conic mirror. In *Proceedings of the 1991 Conference on Computer Vision and Pattern Recognition*, pp. 160-165, June 1991.

- 
- [11] S. Bogner. Introduction to panoramic imaging. In *Proceedings of the IEEE SMC Conference*, pp. 3100-3106, October 1995.
- [12] J.R. Murphy. Application of panoramic imaging to a teleoperated lunar rover. In *Proceedings of the IEEE SMC Conference*, October 1995.
- [13] M. Ollis, H. Herman and S. Singh. Analysis and Design of Panoramic Stereo Vision Using Equi-Angular Pixel Cameras. In Technical report CMU-RI-TR-99-04, Robotics Institute, Carnegie Mellon University, January 1999.
- [14] J. Gluckman, S.K. Nayar and K.J. Thoresz. Real-Time omnidirectional and Panoramic Stereo. In *Proceedings of the 1998 DARPA Image Understanding Workshop*, Monterey, California, 1998.
- [15] S.A. Nene and S.K. Nayar. Stereo with mirrors. In *Sixth International Conference on Computer Vision*, pp. 1087-1094, 1998.
- [16] J. Batlle, E.M. Mouaddib and J. Salvi. A Survey: Recent Progress in Coded Structured Light as a Technique to Solve the Correspondence Problem. In *Pattern Recognition* 31(7), pp. 963-982, July 1998.
- [17] R. Orghidan, J. Salvi and E.M. Mouaddib. Calibration of a structured light-based stereo catadioptric sensor. In *Workshop on Omnidirectional Vision, IEEE International Conference on Computer Vision and Pattern Recognition*, 2003.
- [18] R. Orghidan, E.M. Mouaddib and J. Salvi. Omnidirectional depth computation from a single image. In *IEEE International Conference on Robotics and Automation*, pp. 1234-1239, 2005.
- [19] R. Orghidan. Catadioptric stereo based on structured light projections. PhD thesis, Universitat de Girona, 2006.
- [20] C. Mei. Laser-augmented omnidirectional vision for 3D localisation and mapping. PhD thesis at Ecole Nationale Supérieure Des Mines De Paris Sophia Antipolis, 2007.
- [21] C. Geyer and K. Daniilidis. Equivalence of catadioptric projections and mappings of the sphere. In *First Workshop of Omnidirectional Vision*, pp. 91-96, 2000.
- [22] Y. Yagi. Omnidirectional sensing and its applications. In *IEICE Transactions on Information and Systems*, Vol. E82-D, pp. 568-578, 1999.

- [23] S.S. Lin and R. Bajcsy. The true single view point (SVP) configuration for omnidirectional view catadioptric system using cone mirror. In Technical report MS-CIS-00-24. Computer and Information Science Department, University of Pennsylvania, Philadelphia, USA, 2001.
- [24] T. Svoboda and T. Pajdla, Epipolar Geometry for central catadioptric cameras. In *International Journal of Computer Vision* 49(1), pp. 23-37, 2002.